Biomaterials Advances 177 (2025) 214415

Contents lists available at ScienceDirect

Biomaterials Advances

journal homepage: www.journals.elsevier.com/materials-science-and-engineering-c

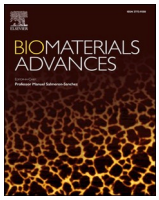

Poly-L-lactic acid nanofiber/polyamidoamine composite hydrogel as novel strategy for in vitro neuroregeneration and neuroprotection

Sofia Treccani [a,1], Irene Bonadies [b,1], Paolo Ferruti [a], Jenny Alongi [a], Enrico Scarpa [c], Paola Laurienzo [b], Maria Grazia Raucci [c], Ines Fasolino [c,*], Elisabetta Ranucci [a,*]

[a] Dipartimento di Chimica, Università degli Studi di Milano, via C. Golgi 19, 20133 Milano, Italy
[b] Institute of Polymers, Composites and Biomaterials – National Research Council (IPCB – CNR), Via Campi Flegrei 34, 80078 Pozzuoli, Italy
[c] Institute of Polymers, Composites and Biomaterials – National Research Council (IPCB – CNR), Viale J. F. Kennedy 54, Mostra D'Oltremare Pad 20, 80125 Napoli, Italy

ARTICLE INFO

Keywords:
Poly-L-lactic acid nanofiber
Polyamidoamine composite hydrogel
In vitro preneuronal cell differentiation
In vitro neuroprotection

ABSTRACT

A purposely designed PLLA/H-AGMA$_{20}$ composite hydrogel incorporating an electrospun poly-L-lactic acid (PLLA) mat in a cell-adhesive polyamidoamine hydrogel (H-AGMA$_{20}$) was investigated as a novel biomaterial with neuroregenerative and neuroprotective properties. A PLLA mat was first functionalized by exposure to ethylenediamine vapors, introducing amine functions through ester group aminolysis, and then impregnated with an α,ω-acrylamide-terminated oligomer (AGMA$_{20}$) aqueous solution. The system was finally cured through UV-induced radical polymerization. The resulting H-AGMA$_{20}$ matrix was covalently grafted onto the PLLA nanofibers since a portion of the AGMA$_{20}$ acrylamide terminals reacted with their surface amine groups, leading to the soft and pliable PLLA/H-AGMA$_{20}$ composite. Biological investigations performed on preneuronal and immune cell lines demonstrated that PLLA/H-AGMA$_{20}$ exhibits promising neuroregenerative properties, effectively promoting both cell proliferation and neuronal differentiation. In addition, the composite demonstrated significant neuroprotective effects in vitro, counteracting neurotoxin 1-methyl-4-phenylpyridinium (MPP$^+$) and proinflammatory agent lipopolysaccharide (LPS)-induced cytotoxicity. These protective results appear to be mediated by modulation of inflammatory pathways, highlighting the combined capacity of biomaterial to support neuronal development while reducing neuroinflammatory damage.

1. Introduction

The use of appropriate in vitro models is fundamental for advancing the understanding of neurotoxicity, a complex phenomenon involving intricate interactions at the molecular, cellular, and tissue levels that are often challenging to investigate in vivo [1]. In this context, hydrogels have emerged as promising platforms due to their inherent biocompatibility and chemical versatility, which can modulate the biological behavior of specific cell types [2]. Their porous architecture facilitates efficient exchange of oxygen, nutrients, and metabolic waste, supporting cell viability and function [3]. Furthermore, their high-water content imparts exceptional softness and viscoelasticity, closely mimicking the mechanical and biochemical properties of the native extracellular matrix [4]. This unique combination of features enables hydrogels to provide both structural support and biologically relevant cues for cell growth and differentiation. Among the different materials used to develop functional hydrogels, polyamidoamines (PAAs) are distinguished as biocompatible and biodegradable water-soluble polymers synthesized by the aza-Michael polyaddition of *prim*- or bis-sec-amines to bisacrylamides. Due to their tunable chemical structure and excellent safety profile, PAAs have proved significant potential in a wide range of biotechnological applications [5–7]. Building on these features, crosslinked PAAs form soft hydrogels can be tailored for specific biomedical applications. Various PAA-based hydrogels have shown strong adhesiveness to different cell types [8,9], including neural cells, which is crucial for neural interface and regeneration strategies [10,11]. In particular, the amphoteric PAA designated AGMA1, synthesized from 4-aminobutylguanidine and 2,2′-bis(acrylamido)acetic acid, stands out among PAAs for its high biocompatibility and bioactivity in both its linear and crosslinked form [12–16]. Notably, AGMA1 hydrogel has demonstrated therapeutic potential in vivo. Indeed, when applied as a conduit in a rat model with a transected sciatic nerve, the hydrogel not

* Corresponding authors.
E-mail addresses: ines.fasolino@cnr.it (I. Fasolino), elisabetta.ranucci@unimi.it (E. Ranucci).
[1] These authors contributed equally.

https://doi.org/10.1016/j.bioadv.2025.214415
Received 14 May 2025; Received in revised form 24 June 2025; Accepted 11 July 2025
Available online 14 July 2025

only supported nerve regeneration but also underwent complete resorption over time [12]. Despite the promising biological properties of AGMA1 hydrogels, their inherent softness affects structural stability, an important factor for maintaining consistent conditions in in vitro studies [12]. To address this limitation, fiber-reinforced hydrogels have been widely studied as a strategy to enhance mechanical strength while preserving biocompatibility, and AGMA1 hydrogels are no exception [17–19]. When reinforced with suitable fibers, AGMA1 can form tough and stitchable membranes, expanding its applicability in biomedical research and device fabrication [20–22]. An essential condition to achieve this result is the existence of amine functions on the fiber surface, which facilitates grafting to the terminal acrylamide groups of the soluble precursor. For example, silk mats derived from degummed raw silk fibers proved efficient in this context due to the reaction of the amine groups of lysine residues [21,22]. Similarly, electrospun poly-L-lactic acid (PLLA) mats surface-functionalized with amine groups by nitrogen plasma treatment became macroscopically compatible with the AGMA1 matrix and remained securely attached to it even after prolonged incubation of the composite hydrogel in water [20]. However, despite its efficacy, the physical treatment of PLLA surface proved complex, and the resulting functionalization was not sufficiently durable, reproducible, or easily scalable for broader production needs.

Electrospun PLLA scaffolds, known for their biocompatibility and biodegradability, have been extensively engineered with tailored surface geometries and chemical functionalization to investigate neuronal cell behavior. These scaffolds are particularly effective in studies involving SH-SY5Y preneuronal cells, a widely recognized in vitro model for exploring the mechanisms underlying neurodegenerative diseases. Functionalization of PLLA fibers with bioactive molecules has been shown to significantly enhance their ability to guide cell adhesion, and differentiation, making them valuable tools for neural tissue engineering [23–26].

Based on inherent bioactivity of the AGMA1 polymer, we developed a composite hydrogel, designated PLLA/H-AGMA20, by reinforcing AGMA1 with electrospun PLLA mats, aiming to create a structurally robust and biologically active scaffold. This composite was specifically designed to modulate SH-SY5Y preneuronal cell behavior in vitro under both physiological and pathological conditions. To ensure strong integration between the PLLA fibers and the AGMA1 matrix, surface amine groups were introduced on electrospun PLLA mats through aminolysis by ethylenediamine vapors [27,28], enabling the formation of tough and macroscopically homogeneous composites. The resulting PLLA/H-$AGMA_{20}$ composite was then evaluated in vitro for its neuroregenerative potential by assessing its ability to support SH-SY5Y preneuronal cell maturation. In addition, its neuroprotective properties were tested by evaluating its effectiveness in mitigating cellular damage in SH-SY5Y and RAW 264.7 immune cells exposed to the neurotoxin 1-methyl-4-phenylpyridinium iodide (MPP^+) and the proinflammatory agent lipopolysaccharide (LPS), respectively.

2. Experimental section

2.1. Materials

Lithium hydroxide monohydrate (>98 %), hydrochloric acid (HCl, 37 %), glyoxylic acid (50 % *w*/w water solution), sulfuric acid (97 %), methyltrichlorosilane (99 %), Phosphate Buffered Saline (PBS), lipopolysaccharide (LPS) from *Escherichia coli* (O111:B4), Griess reagent and 1-methyl-4-phenylpyridinium iodide (MPP^+) were supplied by Sigma-Aldrich (Milan, Italy) and used as received. 4-aminobutylguanidine sulphate (95 %) was purchased from Enamine (Riga, Latvia); acrylonitrile (99.5 %) and ethylenediamine (EDA) (≥ 98 %) were supplied by Fluka (Charlotte, NC).

2.2. Synthesis of 2,2′-bis(acrylamido)acetic acid

A mixture of glyoxylic (25.2 g, 50 % water solution, 0.17 mol) and sulfuric acid (69.1 g, 0.68 mol) was prepared by adding glyoxylic acid dropwise to sulfuric acid kept at 0 °C in a water/ice bath. The cold acid mixture was then dropped slowly to an acrylonitrile (26.4 g, 0.50 mol) and copper acetate (10 mg) mixture placed in an acetone/ice bath at −4 °C. The addition rate was adjusted to maintain the reaction temperature between 0 and 10 °C. After completing the addition, the mixture was kept under stirring for another 2.5 h, allowing it to gradually warm up to room temperature. The resulting yellowish, viscous solution was slowly poured to cold water (120 mL, 4–5 °C) to give a white precipitate, which was kept at 4 °C overnight. After this time, the raw product was retrieved by filtering, then washed three times by dispersing in cold water (4–5 °C) for 20 min and then filtering. The final product was dried to constant weight under reduced pressure, giving a fine white powder that was analyzed by nuclear magnetic resonance spectrometry, ^{1}H NMR (Fig. S1 in Supporting Information), and acid-base titration. Yield = 24.25 g (72 %), purity = 98 %.

2.3. Synthesis of AGMA oligomers with acrylamide terminals

2.3.1. AGMA20

Agmatine sulphate (4.85 g, 0.021 mol) and lithium hydroxide monohydrate (0.87 g, 0.021 mol) were added to an aqueous solution obtained by mixing 2,2′-bis(acrylamido)acetic acid (5.00 g, 0.025 mol) and lithium hydroxide monohydrate (1.07 g, 0.025 mol) in water (12.0 mL). The reaction mixture was stirred and heated to 50 °C until fully dissolved, then kept at 25 °C in the dark for 4 days. After this time, a 1 mL aliquot of the solution was acidified to pH 4.5 using 6 M HCl, then freeze-dried. The resulting solid was analyzed by ^{1}H NMR (Fig. S2). The remaining portion of the reacting mixture was acidified to pH 7 with 6 M HCl and used in the subsequent hydrogel synthesis without further treatment.

AGMA oligomers with different amounts of terminal acrylamide groups were prepared following the same procedure adopted for $AGMA_{20}$, by using the amounts of the reagents shown in Table 1.

2.4. Synthesis of H-AGMA hydrogels

2.4.1. H-AGMA20

The H-$AGMA_{20}$ hydrogel samples were obtained in the form of sheets using as a mold two silanized 2 mm thick glass plates separated by a 0.5 mm thick silicone frame with an internal volume of 25 mm × 50 mm × 0.5 mm. Before use, the glass plates were silanized using methyltrichlorosilane. The hydrogel samples were obtained by first injecting an $AGMA_{20}$ solution (0.5 mL) in the mold, and then irradiating the mold 30 min per side using a 250 W HG200 Ultra UV lamp (Jelosil S.r.l., Vimodrone, Milan, Italy) (emission range 315–400 nm) positioned 15 cm away. The thickness of the hydrogel samples obtained using this procedure averaged 0.42 ± 0.02 mm, as determined using a Dino-Lite Edge digital microscope (Dino-Lite Europe, Almere, The Netherlands) equipped with the DinoXcope software.

For comparison purposes, H-AGMA10, H-AGMA20 and H-AGMA30 hydrogels were prepared from the corresponding oligomers using molds of different size and shape.

Table 1
Amounts of the reagents used in the synthesis of AGMA oligomers.

	BAC[a])		Agmatine sulfate		$LiOH·H_2O$		H_2O
	(g)	(mmol)	(g)	(mmol)	(g)	(mmol)	(mL)
$AGMA_{10}$	5.05	25	5.41	22.5	2.04	47.5	12
$AGMA_{20}$	5.05	25	4.80	20.0	1.93	45.0	12
$AGMA_{30}$	5.05	25	4.20	17.5	1.82	42.5	12

[a] 2,2′-bis(acrylamido)acetic acid.

2.5. Electrospinning of PLLA fibers

PLLA (Ingeo™ 4032D 0.7 mol% L-isomer, molar mass: 2.1 × 10^5 g mol^{-1} and polydispersity (PDI) = 1.7) was supplied by NatureWorks LLC (Minneapolis, Minnesota, USA); all solvents were reagent grade. The PLLA solution (10 % *w/v* in chloroform/dimethylformamide 90/10) was electrospun using an electrospinning setup NF103 MECC Co., Ltd. (Fukuoka, Japan) equipped with a 0.55 mm (inner diameter) needle and a plate collector, at a flow rate of 3 mL h^{-1}, room temperature and 30 % relative humidity. The voltage and distance between the needle tip and the collector were 30 kV and 25 cm, respectively. Fibers were collected for at least 2 h, thus obtaining a mat with a thickness of about 100 μm (measured using a digital micrometer).

2.6. Functionalization of the PLLA surface

EDA (10 mL) was poured into an open 100 mL beaker. A PLLA mat, 100 μm thick, was placed on a metal grid positioned 50 mm above the liquid, exposing it to EDA vapors for 1 min on each side. The mat was then washed with ultrapure water to remove traces of adsorbed EDA. After EDA treatment, a PLLA strip (12 mg) was impregnated with a 0.4 % *w*/w ninhydrin aqueous solution and maintained at 55 °C for 1 h [29]. Ninhydrin reacts with amines to form a colored complex - Ruhemann's purple - enabling visualization of functionalization. The PLLA surfaces were therefore spectrophotometrically analyzed following the ISO11664 standard using a YS3010 Handheld Spectrophotometer (3nh Global, Guangzhou, China) equipped with the SQCX software. The following CIELAB color space parameters were obtained: brightness, L^*, ranging from 0 (black) to 100 (white); chromaticity coordinates a^* (green-red axis), and b^* (blue-yellow axis); color change (ΔE^*), given by Eq. (1), which quantifies perceptual differences in color given:

$$\Delta E^* = \sqrt{(\Delta L^*)^2 + (\Delta a^*)^2 + (\Delta b^*)^2} \quad (1)$$

2.7. Synthesis of the PLLA/H-AGMA$_{20}$ composite hydrogel

The PLLA/H-AGMA$_{20}$ samples were synthesized using the same glass mold used for the preparation of the H-AGMA$_{20}$ hydrogel. An aliquot of the AGMA$_{20}$ oligomer solution (0.3 mL) was first injected in the open mold filling the void volume within the frame. A 25 mm × 50 mm × 0.1 mm PLLA mat (24 mg) was then inserted in the mold and slightly compressed to facilitate impregnation with the AGMA$_{20}$ solution. An additional aliquot of the AGMA$_{20}$ solution (0.3 mL) was then added; the mold closed with a second glass plate and blocked, taking care to let out the excess solution. The curing reaction was then initiated by UV irradiation, following the procedure used for the plain H-AGMA$_{20}$ hydrogel. The final composite sample was gently detached from the glass plates and soaked in water for 2 h. The thickness of the composite hydrogel obtained using this procedure averaged 0.49 ± 0.02 mm, as determined using a digital microscope. All PLLA/H-AGMA$_{20}$ samples were stored in fresh water. The synthetic process adopted to obtain the PLLA/H-AGMA$_{20}$ composite hydrogels is depicted in Fig. S3.

2.8. Structural characterization

Unfunctionalized and EDA-functionalized PLLA mats before and after washing were analyzed by attenuated total reflectance (ATR) Fourier transform-infrared spectroscopy (FT-IR). FT-IR/ATR spectra were recorded at room temperature, in the 4000–600 cm^{-1} wavenumber range, with 256 scans and 4 cm^{-1} resolution, using a Jasco FT-IR/FIR spectrophotometer (Milan, Italy), equipped with a ZnSe crystal.

2.9. Scanning electron microscopy

The morphology of PLLA mats and PLLA/H-AGMA$_{20}$ was analyzed using a Zeiss field-emission scanning electron microscope (FE-SEM), model ZEISS-SIGMA 300 operating at 10.8 mm working distance and 5 kV beam voltage. Samples (5 mm × 5 mm) with a 4 nm thick platinum metallization were examined on both the top surface and the cross-section, which was prepared through brittle fracture.

2.10. Tensile tests

The mechanical properties of the PLLA/H-AGMA$_{20}$ composite hydrogel and the PLLA mat were analyzed by tensile tests performed at room temperature by using a 5564 Instron (Turin, Italy) equipped with a 100 N cell load, at a crosshead speed of 5 mm min^{-1}. Tests were performed on five specimens in the hydrated form, immediately after removal from water; the specimens were prepared by cutting 50 mm large strips from electrospun mats and composite hydrogel membranes. A gauge length of 10 mm was used, and the thickness of the samples was measured with a digital micrometer. The mechanical response of samples is expressed in terms of nominal stress and strain, where the nominal stress is calculated as the ratio of force and initially measured cross-section, the nominal strain is calculated from the ratio of the distance changing between two grips in the tensile testing machine and its initial distance.

2.11. Thermogravimetric analysis

The thermal stability of the PLLA mat, H-AGMA$_{20}$ and PLLA/H-AGMA$_{20}$ was assessed by thermogravimetric analysis (TGA) in nitrogen and air from 30 to 800 °C range, at 10 °C min^{-1} heating rate, with a 50 mL min^{-1} gas flow, using a TGA 2 Star System (Mettler-Toledo, Milan, Italy). All samples were dried in isothermal conditions at 100 °C for 3 min prior to the heating run.

2.12. In vitro biological tests

2.12.1. Cell culture

For the biological analysis on the neuroprotective and anti-inflammatory properties of PLLA/H-AGMA$_{20}$, two cell lines were used as SH-SY5Y cells (neuroblastoma cell line derived from a metastatic bone tumor from a 4-year-old cancer patient) and RAW 264.7 cells (macrophage cell line from a male mouse) purchased from Sigma Aldrich (Milan, Italy).

Cells were cultured in Dulbecco's modified Eagle medium (DMEM), supplemented with 10 % fetal bovine serum (GIBCO), an antibiotic solution (streptomycin 100 μg mL^{-1} and penicillin 100 U mL^{-1}, Sigma Chem. Co) and 2 mM L^{-1} glutamine. To ensure sterility, the substrates were sterilized under UV light for 2 h (h), followed by incubation in an antibiotic solution (streptomycin 100 μg mL^{-1} and penicillin 100 U mL^{-1}, Sigma Chem. Co). Cells were then seeded onto PLLA/H-AGMA$_{20}$ and grown up to 14 days, with the culture medium being replaced every 3 days. Cells grown on flat plates were used as the control group. Additionally, neuronal cell behavior on PLLA fibers alone was also investigated and extensively documented in previous studies [23,25,26].

2.12.2. In vitro assessment of SH-SY5Y cell viability and adhesion

SH-SY5Y cells were seeded onto PLLA/H-AGMA$_{20}$ at a density of 1.5 × 10^4/well in a 48 multiwell (MW) plate and incubated at 37 °C with 5 % CO_2. Cell viability after cell-substrate interaction was assessed at different time points (1, 3, 7 and 14 days) using AlamarBlue® (Bio-Rad Laboratories, Inc., Italy), a widely used reagent that measures metabolic activity as an indicator of cell vitality and proliferation. At each point, the cell culture medium was removed, and a 10 % (*v*/v) AlamarBlue® solution was added to each well, followed by incubation at 37 °C for 3 h. The reduction of resazurin to resorufin by metabolically active cells correlates directly with cell viability and proliferation, allowing for a quantifiable measure of cell vitality [29]. This assay provides a reliable

assessment of cellular metabolism, reflecting the dynamic interaction between the cells and the PLLA/H-AGMA20 substrate. The optical density of the resorufin product was measured using a UV–Visible spectrophotometer (Victor X3 Multilabel Plate Reader, Perkin Elmer, Milan, Italy) at wavelengths of 570 and 600 nm. Additionally, cell adhesion on PLLA/H-AGMA$_{20}$ was evaluated from a qualitative point of view through fluorescence analysis. To this end, SH-SY5Y cells were seeded onto substrates placed in a 24 MW plate (2×10^4 cells/well) or on flat surfaces used as control. After 24 h seeding, cells were fixed with a solution containing 4 % (*w/v*) paraformaldehyde (PFA) (Sigma-Aldrich) for 24 h at 4 °C. Later, samples were washed thrice with Phosphate Buffered Saline (PBS) 1× and permeabilized with 0.1 % Triton X-100 in 0.1 % bovine serum albumin (BSA, Sigma Aldrich) for 1 h. After permeabilization, samples were washed thrice with PBS 1× and stained with FITC (fluorescein 5(6)-isothiocyanate)-conjugated phalloidin (Thermo Fisher Scientific, Waltham, Massachusetts, USA) solution for 1 h. Later, samples were washed, and nuclei were counterstained with 10 μg mL^{-1} 4′,6-diamidino-2-phenylindole (DAPI) (Molecular Probes®, Thermo Fisher Scientific). The samples were washed with PBS thrice and cell images wer acquired with fluorescence microscope at magnification 10× (JuLI™ Stage by NanoEntek).

2.12.3. SH-SY5Y cells differentiation

SH-SY5Y neuronal differentiation was tested through an immunofluorescence technique performed using FITC-conjugated GAP-43 (Growth Associated Protein 43) antibody (Thermo Fisher Scientific) as marker of neuron maturation. For GAP-43 expression quantification, 2×10^4 cells/well were seeded and cultured onto PLLA and PLLA/H-AGMA$_{20}$ in a 24 MW plate using basal culture medium for 7 and 14 days. Then, cell fixation and permeabilization were performed as described earlier in cell adhesion assay. Later, the neuronal specific marker protein FITC-conjugated GAP-43 (1:100 dilution) was added to each sample and incubated overnight at 4 °C. After three washes in PBS (Phosphate Buffered Saline), the cytoskeleton was stained with anti-Phalloidin-ATTO 594 (Sigma Aldrich) solution (1:200) for 1 h. Finally, nuclei staining was performed through DAPI incubation for 10 min at 37 °C. The samples were washed with PBS thrice and cell images acquired with fluorescence microscopes at magnification 10× (JuLI™ Stage by NanoEntek and Leica TCS SP8 confocal microscope, Germany). Image analysis was performed using the ImageJ software (ImageJ 1.44 which uses Java 1.6 in 64-bit mode) to extrapolate fluorescence intensity. The fluorescence intensity was normalized to the number of cells per surface by subtracting the background intensity from the cell intensity and was expressed as the mean fluorescence intensity.

2.12.4. SH-SY5Y-response to MPP$^+$ stimulation

To evaluate the neuroprotective properties of PLLA/H-AGMA$_{20}$ to prevent SH-SY5Y cell death induced by MPP$^+$ exposure, a widely used neurotoxin in in vitro models for assessing neurotoxicity. SH-SY5Y cells (1.5×10^4/well) were seeded on PLLA/H-AGMA$_{20}$ in a 48 MW plate for 7 days. After this time, the cells were stimulated with MPP$^+$ (1.5 mM) for 24 h to induce neurotoxic damage, and cell survival was evaluated using the AlamarBlue® assay as previously described.

MPP$^+$ is known to cause cell death in dopaminergic neurons, and TLR-4 signaling is recognized as a key pathway involved in the inflammatory response triggered by MPP$^+$ exposure [30]. To assess the impact of PLLA/H-AGMA20 on inflammation, we measured changes in TLR-4 expression through fluorescence analysis. Following cell fixation and permeabilization performed as previously described, cells (2×10^4/well) were incubated overnight with FITC conjugated rabbit anti-TLR-4 polyclonal antibody (Thermo Fisher Scientific) using a 1:200 dilution, cytoskeleton was stained with anti-Phalloidin-ATTO 594 (Sigma Aldrich) solution (1:200) for 1 h and counterstained with DAPI at concentration of 10 μg mL^{-1} for 10 min at 37 °C for nuclei detection. Cells were observed using a confocal laser-scanning microscope at 10× magnification (Leica TCS SP8 confocal microscope, Germany). Image analysis was performed as previously described for GAP-43 expression.

2.12.5. SH-SY5Y and RAW 264.7 inflammatory response

Firstly, RAW 264.7 viability was measured using AlamarBlue® (Bio-Rad Laboratories, Inc. Italy) after 7 days of cell-material interaction and 24 h stimulation with the flogistic agent (LPS 10 μg mL^{-1}). Later, inflammatory marker production was quantified on SH-SY5Y and RAW 264.7 seeded onto PLLA/H-AGMA$_{20}$ and stimulated with MPP+ and LPS for 24 h, respectively. Briefly, cells were plated and grown for 7 days in a 12 MW plate at density of 5×10^4 cells/well. Following this incubation period, the cells were exposed to MPP$^+$ (1.5 mM) or LPS (10 μg mL^{-1}) for 24 h, both in the presence and absence of PLLA/H-AGMA$_{20}$. After this time, cell supernatants were collected. For nitrite levels production, 100 μL supernatant were incubated into a 96 MW plate with an equal volume of Griess reagent (Sigma Aldrich, Milan, Italy) and the absorbance was measured at 550 nm after 1 h incubation at room temperature using a fluorescent microplate reader (VICTOR X3, 156 PerkinElmer, Milan, Italy). Furthermore, IL-1β and IL-10 levels were quantified on cell supernatants using commercial ELISA kits (Elabioscience) following manufacturer's instructions.

2.12.6. Inhibition of neuroinflammatory pathways in SH-SY5Y cells

The inhibition of inflammatory signaling in SH-SY5Y was investigated by assessing specific pathways, including Caspase-1 cascade and the expression of the neurotrophic factor beta-nerve growth factor (β-NGF), using fluorescence analysis. To this end, SH-SY5Y cells (2×10^4 cells/well) were seeded onto PLLA/H-AGMA20 composites and PLLA alone in a 48 MW plate and cultured for 7 days. After this time, cells, with or without stimulation by 1.5 mM MPP$^+$ for 24 h, were fixed and permeabilized as previously described.

Later, cells were incubated overnight with rabbit anti-Caspase-1 polyclonal antibody (Proteintech) using a 1:50 dilution or rabbit polyclonal anti-beta NGF (Arigo Biolaboratories Corp.) using a 1:500 dilution at 4 °C followed by incubation with FITC-goat anti-rabbit IgG antibody (1:80, Sigma Aldrich, Milan, Italy) for 1 h at room temperature. The cytoskeleton was stained with anti-Phalloidin-ATTO 594 (Sigma Aldrich) solution (1:200) for 1 h, followed by nuclear counterstained with DAPI at concentration of 10 μg mL^{-1} for 10 min at 37 °C. After staining, the samples were washed three times with PBS. Fluorescence imaging was performed using a JuLI™ Stage (NanoEntek) at 10× magnification. Image analysis was performed using ImageJ software (version 1.44, running on Java 1.6 in 64-bit mode), as previously described.

2.13. Statistical analysis

Statistical analyses were performed using GraphPad Prism®, version 8.00 (GraphPad Software, La Jolla, California, USA). Data were analyzed using a Student's *t*-test, Two-way ANOVA and Sidak's multiple comparisons test as appropriate. The results are expressed as mean ± standard deviation (SD). Values of $p < 0.05$ were considered significant.

3. Results and discussion

3.1. Synthesis of H-AGMA hydrogels

To select the best hydrogel matrix to be used in the synthesis of the PLLA-reinforced composites, plain H-AGMA hydrogel samples were prepared under the same curing conditions of the PLLA/H-AGMA$_{20}$ composite. H-AGMA hydrogels were synthesized in two steps. The first step was the synthesis of the α,ω-acrylamide-terminated oligomeric precursors, designated AGMA$_{10}$, AGMA$_{20}$ and AGMA$_{30}$, obtained by the reaction of 2,2′-bis(acrylamido)acetic acid with 4-aminobutylguanidine in a 1:0.9, 1:0.8 and 1:07 M ratio, respectively – the synthesis of AGMA$_{20}$ is shown Scheme 1a. These oligomers were obtained as a 50 wt% aqueous solution. Their structure was confirmed through ^{1}H NMR

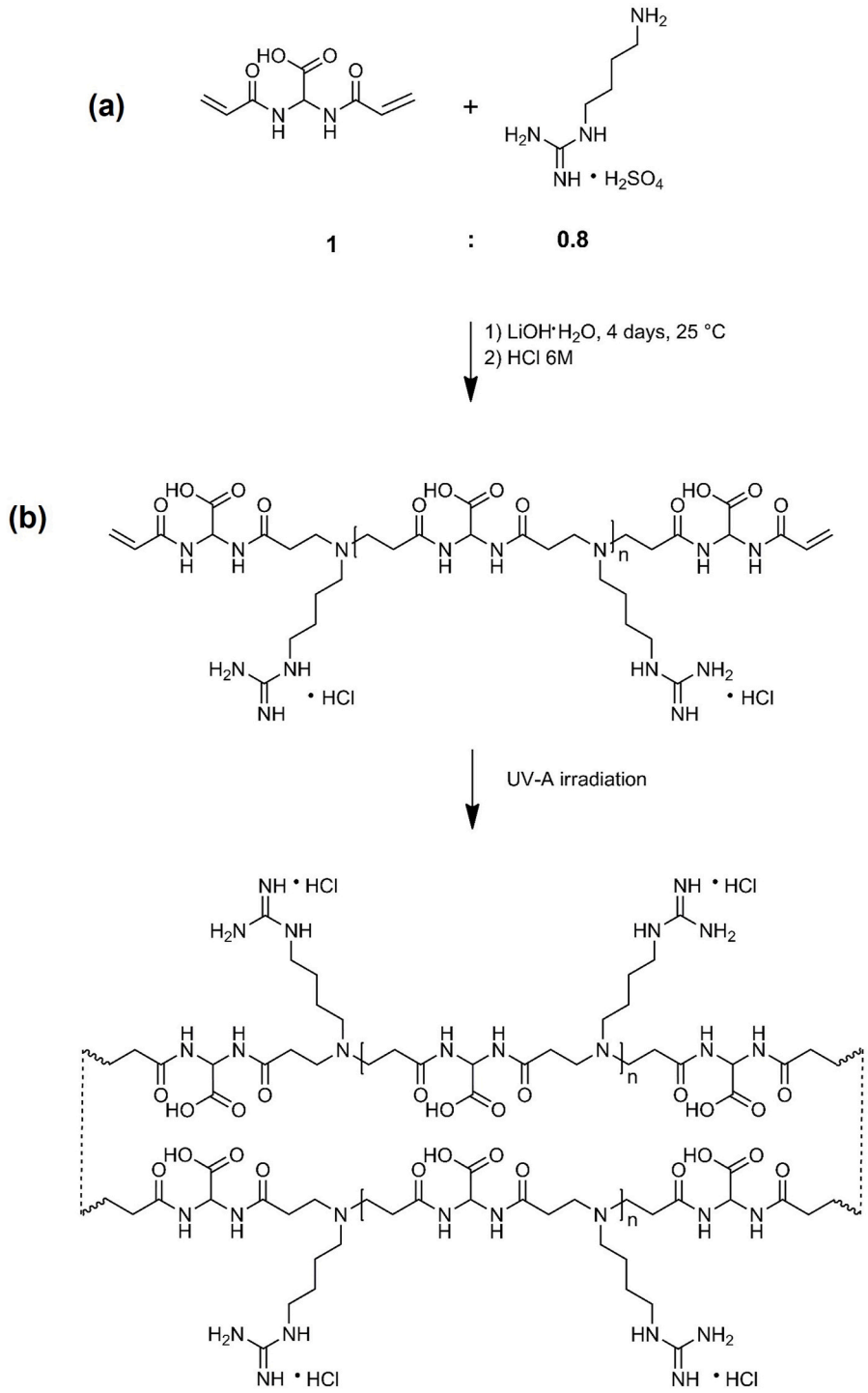

Scheme 1. Synthesis of the H-AGMA$_{20}$ hydrogel: synthesis (a) and cross-linking (b) of the AGMA$_{20}$ oligomer. Number of the repeat units, $n = 6$, from ^{1}H NMR (Fig. S2).

spectroscopy. As an example, the ^{1}H NMR spectrum of AGMA$_{20}$ is shown in Fig. S2. The second step was the UV-initiated radical polymerization of the AGMA oligomers conducted at pH 7 (Scheme 1b). The cross-linking reaction produced hydrogel sheets approximately 420 μm thick when fully swollen, exhibiting varying degrees of softness and fragility. Based on visual inspection, H-AGMA$_{10}$ was overly soft and pliable, while H-AGMA$_{30}$ was brittle and tended to crumble upon swelling (Fig. S4c and S4d). H-AGMA$_{20}$ offered the best balance of mechanical properties and ease of handling (Fig. S4a and S4b), and was therefore selected as the preferred hydrogel matrix for combination with the PLLA reinforcing mat.

3.2. Functionalization and characterization of PLLA nanofibers

PLLA mats with a thickness up to 100 μm were produced through electrospinning following optimization of the process parameters. In their native state, the PLLA mats were water-unwettable and incompatible with the aqueous AGMA$_{20}$ oligomer solution, likely due to their inherent hydrophobicity, which impeded effective impregnation. To address this limitation, the mats were exposed to ethylenediamine

(EDA) vapors, to introduce amine groups onto the PLLA surface via an aminolysis reaction, a widely used method for modifying the surface of polyesters [31]. The average fiber diameters of the untreated PLLA mat and the EDA-treated PLLA mat (after water washing) were 2.231 ± 0.431 μm and 1.856 ± 0.257 μm, respectively. SEM micrographs and the corresponding diameter distribution are reported in Fig. S5.

The effectiveness of the aminolysis reaction was validated through a ninhydrin staining test [32]. The color changes observed in the PLLA samples were spectrophotometrically analyzed to determine the CIELAB chromatic parameters. The results, presented in Fig. 1c and d, show a decrease in brightness, L^*, a significant increase in the b^* coordinate (from −0.19 to 0.39; blue-yellow), and an even more substantial increase in the a^* coordinate (from 0.56 to +5.52; red axis) for EDA-treated PLLA. This pronounced shift towards redness confirms the presence of amines on PLLA surface.

Following EDA treatment, the water wettability of the PLLA mat increased significantly. In fact, while the contact angle for untreated PLLA was approximately 132° (Fig. 1a with inlet), consistent with literature reports [33], the EDA-treated PLLA was rapidly wetted, and the resultant contact angle negligible. Notably, the EDA-treated PLLA mat was transparent (Fig. 1b), as evidenced by the visibility of the blue tweezers in the background, in contrast to the untreated mat, which remained opaque (Fig. 1a).

The effect of the exposure to EDA vapors on the surface morphology of the PLLA mat was investigated by SEM and compared to that of the virgin mat. Fig. 1e and f show the morphologies of untreated and EDA-treated PLLA mats at 1000× and 2500× magnifications, respectively. The PLLA mats were formed by randomly distributed fibers, homogenous in size and with a smooth surface texture. Following EDA treatment and washing, the PLLA mat retained the morphology of the neat PLLA mat, with no observable structural changes detected.

Elemental analysis of the functionalized PLLA mat, carried out using Energy Dispersive X-ray Spectroscopy (EDX), confirmed the presence of carbon and oxygen – elements abundant on the PLLA surface – but did not detect nitrogen (Fig. 1g). This limitation is likely due to the low surface concentration of amine groups combined with the low energy (0.392 keV) of nitrogen's characteristic Kα X-ray, which makes its detection by EDX challenging.

3.3. Synthesis and physico-chemical characterization of the PLLA/AGMA$_{20}$ composite hydrogel

The multistep procedure used to synthesize the PLLA/H-AGMA$_{20}$ composite hydrogel, as described in detail in the Experimental section, gave a flexible, pliable, and macroscopically homogeneous PLLA/H-AGMA$_{20}$ composite hydrogel about 490 μm thick when fully hydrated (Fig. S6a,b), which could stand several weeks immersed in water without any evidence of detachment of PLLA fibers from the hydrogel matrix (Fiber S6c). In the dry state, the composite was composed of 8 wt % PLLA and 92 wt% H-AGMA$_{20}$, therefore its water uptake capacity was comparable to that of pure H-AGMA20, reaching values close to 300 %. PLLA/H-AGMA20, as H-AGMA20 does, showed complete reversibility in multiple swelling/drying cycles (Fig. S7), with excellent resistance to the osmotic stress encountered in the process.

Scanning electron microscopy (SEM) analysis of the fracture surface of PLLA/H-AGMA$_{20}$ (Fig. 2a) confirmed the anticipated sandwich-like structure, consisting of two H-AGMA$_{20}$ hydrogel layers 46.7 ± 1.1 μm and 50.5 ± 0.9 μm thick, respectively, enclosing a 33.9 ± 2.8 μm PLLA layer. Moreover, PLLA/H-AGMA20 samples could stand several weeks immersed in water without any evidence of detachment of PLLA fibers from the hydrogel matrix.

The morphological analysis of the fracture surface of PLLA/H-AGMA$_{20}$, carried out by SEM (Fig. 2a), revealed that PLLA fibers appeared perfectly integrated into the H-AGMA$_{20}$ hydrogel matrix, with no visible detachment areas. This result supports the hypothesis that covalent bonds are formed between the PLLA fibers and the hydrogel matrix, highlighting their crucial role in reinforcing the composite material. To definitively confirm that H-AGMA$_{20}$ was covalent linked to the PLLA surface, a virgin PLLA mat (not exposed to EDA vapors) was first impregnated with an AGMA$_{20}$ oligomer solution and then cured following the same procedure as for the PLLA/H-AGMA$_{20}$ composite. The resultant material was macroscopically uneven and exhibited complete separation of the hydrogel from the fiber component after water swelling, as revealed by both optical (Fig. 2b) and scanning electronic (Fig. 2c) microscopies.

The PLLA/H-AGMA$_{20}$ composite was characterized by FT/IR-ATR spectroscopy and its spectrum compared to those of its constituents (Fig. S8). Notably, only the diagnostic bands of the hydrogel matrix were detected, consistent with its role as the primary constituent of the composite (8 wt% PLLA, 92 wt% H-AGMA$_{20}$ in its dry state).

The mechanical performance in terms of Young's modulus, maximum stress and strain at break of the PLLA/H-AGMA20 composite hydrogel was analyzed by means of tensile properties and compared to those of the PLLA mat and plain H-AGMA20 hydrogel.

Tensile parameter analysis, (Table 2), confirms that the PLLA mat effectively reinforced the H-AGMA20 hydrogel through covalent bonding, enhancing its structural integrity. As shown in Table 2, the H-AGMA20 hydrogel was a relatively rigid material, yet exhibited a low

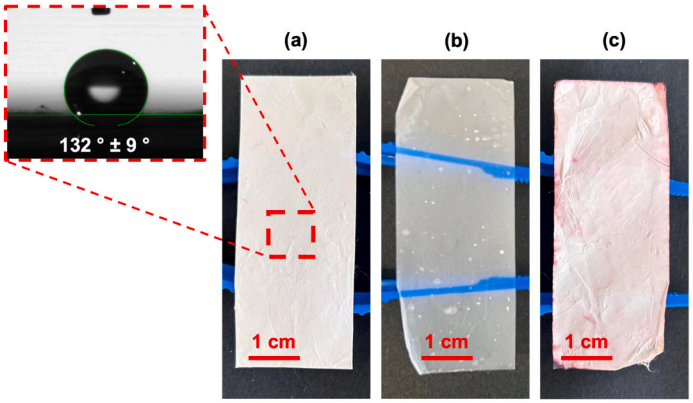

(d)

	PLLA (a)	EDA-treated PLLA after ninhydrin staining (c)
L*	95.04	90.68
a*	0.56	**5.52**
b*	-0.19	0.39
Simulated color		
ΔE*	6.63	

Fig. 1. Untreated PLLA mat (a); EDA-treated PLLA mat after washing with water before (b) and after (c) ninhydrin staining; CIELAB chromatic parameters: brightness (L^*), a^* (green-red axis) and b^* (blue-yellow axis) coordinates (d). Insert to (a) shows the contact angle of untreated PLLA mat. The PLLA sample shown in 3b is notably transparent, as evidenced by the visibility of the blue tweezers in the background. SEM micrographs of untreated PLLA mat (e) and EDA-exposed PLLA mat after washing (f). SEM micrograph with EDX color analysis of EDA-exposed PLLA mat after washing (g). (For interpretation of the references to color in this figure legend, the reader is referred to the web version of this article.)

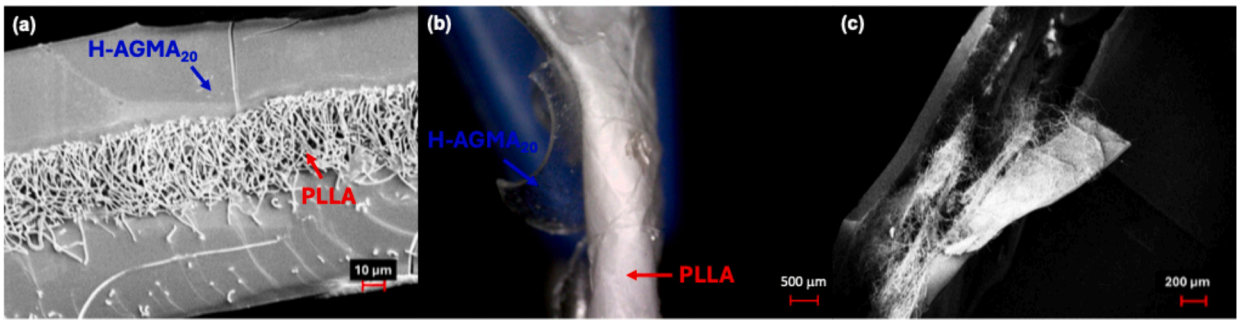

Fig. 2. SEM micrographs of fragile fracture surfaces of PLLA/H-AGMA$_{20}$ (a). Optical microscope (b) and SEM (c) micrographs of an H-AGMA$_{20}$ hydrogel with an embedded PLLA mat, not previously exposed to EDA vapors.

Table 2
Tensile parameters of PLLA/H-AGMA$_{20}$ and its constituents.[a)]

Sample	Young modulus (MPa) ± SD	Stress max (MPa) ± SD	Strain at break (%) ± SD
H-AGMA$_{20}$	0.3 ± 0.1	0.04 ± 0.01	0.01 ± 0.06
PLLA	88.52 ± 31.96	3.89 ± 0.49	215.78 ± 23.58
PLLA/H-AGMA$_{20}$	47.82 ± 17.89	2.2 ± 0.38	39.96 ± 9.03

[a] All values are reported as the average of five measurements ± standard deviation (SD).

elastic modulus (0.3 MPa, Table 2). It endured an ultimate tensile strength of 0.10 N and a maximum stress of 0.04 MPa before failing. However, this reinforcement also resulted in a decrease of the tensile properties of the composite, especially strain at break, primarily due to the relatively low PLLA content in the composite (8 wt% in its dry state and 4 wt% in its hydrated state). This embrittlement of the fibrous mat can be ascribed to the strong interconnection with the hydrogel matrix, as observed in SEM imaging (Fig. 2), which restricts fiber alignment under stress. This behavior is noticeable by analyzing the stress-strain curves (Fig. S9) for both PLLA/H-AGMA20 and PLLA. An initial linear elastic behavior characterized by minimal deformation, due to the interwoven structure of the fibrous mat network (Fig. 2a) is evident. Once the inter-fiber junction rupture occurred, further deformation on the mat was unrecoverable. After the elastic deformation, the PLLA/H-AGMA20 composite extended uniformly along its entire length without significant necking until failure. On the contrary, the PLLA mat specimen exhibited high tensile elongation accompanied by significant reduction in the width as fibers slid over one another and aligned in the direction of the applied tensile load, ultimately leading to complete failure [34].

The thermal stability of PLLA/H-AGMA$_{20}$ was investigated by means of TGA both in inert - nitrogen- and oxidant – air - atmosphere and compared with that of both constituents. The TG thermograms and the collected results are shown in Fig. 3 and Table 3, respectively. In accordance with the literature reports, PLLA had its maximum weight loss around 350 °C both in nitrogen and in air and its decomposition occurred in one step [35]. As also demonstrated in a previous study [21], H-AGMA$_{20}$ decomposed in nitrogen via a multimodal mechanism involving four distinct weight loss steps: two occurring within the 160–250 °C range, and the other two centered at 235 °C and 304 °C (Fig. 3a). Notably, the decomposition onset temperature at 10 % weight loss ($T_{onset10\%}$) was significantly lower than that observed in the hydrogel composite (190 °C vs 197 °C). In air, the H-AGMA$_{20}$ thermogram overlapped that in nitrogen in the 100–250 °C range (Fig. 3b). Beyond this temperature range, the TG curve in air exceeded that observed in nitrogen, consistent with previous findings for polyamidoamines. In fact, in between 300 and 600 °C, H-AGMA$_{20}$ underwent oxidation producing a thermally stable carbonaceous char thanks to the phenomenon of intumescence [36]. The TG profile of PLLA/H-AGMA$_{20}$ closely resembled that of plain H-AGMA$_{20}$ in both nitrogen and air, consistent with the hydrogel matrix being the primary component of the composite (8 wt% PLLA, 92 wt% H-AGMA$_{20}$ in its dry state). To

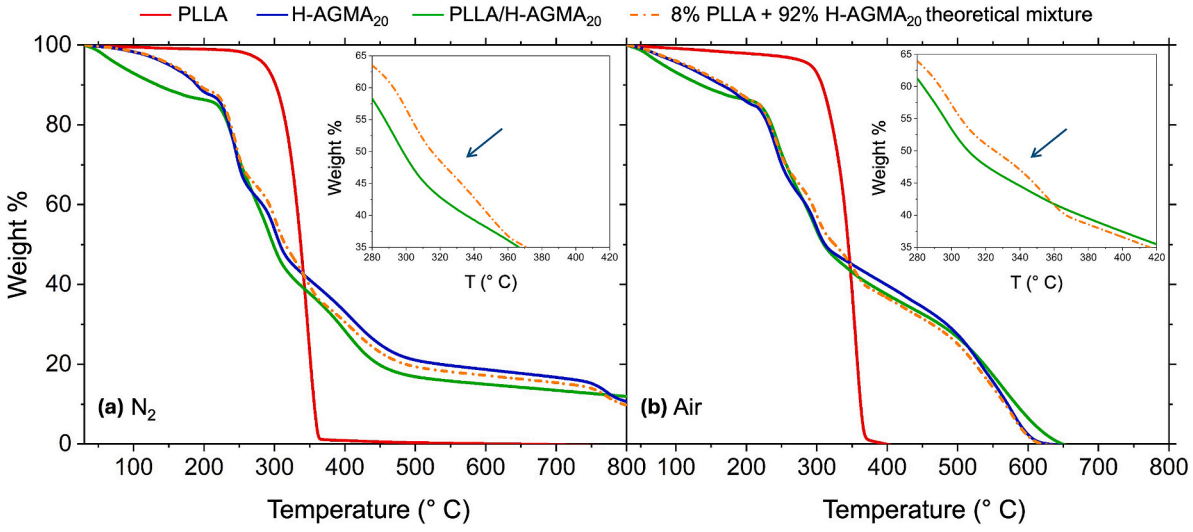

Fig. 3. TG thermograms in nitrogen (a) and air (b) of the PLLA mat (red), H-AGMA$_{20}$ (blue), PLLA/H-AGMA$_{20}$ (green). The theoretical curves (orange) were calculated from the additive contribution of each component. (For interpretation of the references to color in this figure legend, the reader is referred to the web version of this article.)

Table 3
Thermogravimetric data of PLLA, H-AGMA$_{20}$ and PLLA/H-AGMA$_{20}$ in nitrogen and air.

Sample	$T_{onset10\%}$ (°C)	T_{max1} [a)] (°C)	T_{max2} [a)] (°C)	T_{max3} [a)] (°C)	T_{max4} [a)] (°C)	Residual mass fraction at 800 °C (%)
Nitrogen						
PLLA	302	347	–	–	–	0
H-AGMA$_{20}$	190	189	244	302	411	11
PLLA/H-AGMA$_{20}$	134	59	243	293	404	12
Air						
PLLA	307	354	–	–	–	0
H-AGMA$_{20}$	165	191	242	300	578	0
PLLA/H-AGMA$_{20}$	136	64	243	294	568	0

[a] Determined from the 1st derivative TG curve.

highlight possible differences, the theoretical curves (dotted orange curves in Fig. 3), calculated from the additive contribution of each component, were compared with the experimental thermograms of the composite. Interestingly, the theoretical curves simulating the thermal experiments conducted in both nitrogen and air show slight inflections around 350 °C, which are attributed to the decomposition of neat PLLA. These inflections are absent in the composite thermograms (see inlets), confirming that PLLA/H-AGMA$_{20}$ is not merely a simple mixture but a true composite, with its components fully integrated through covalent bonding.

3.4. PLLA/H-AGMA$_{20}$ biological properties

3.4.1. Effect of PLLA/H-AGMA$_{20}$ on SH-SY5Y viability, adhesion and differentiation

Traditionally, numerous studies on neurodegenerative processes were realized on two-dimensional (2D) cell cultures models. While these systems are easy to use and widely adopted, they fall short of reproducing the complexity of the in vivo environment. In contrast, recent studies have highlighted the potential of biologically inspired scaffolds, such as hydrogel matrices, to better mimic the extracellular matrix and promote more physiologically relevant neuronal behavior. These scaffolds not only enhance the differentiation of preneuronal cells into dopaminergic-like neurons (DLNs), but also help modulate cell proliferation, a key factor in neuroregeneration [23,37]. It is well recognized that cell proliferation and differentiation display a striking inverse relationship: precursor cells carry out division before transitioning into differentiated state, while terminal differentiation is typically associated with the arrest of proliferation [38]. This interplay is critical for the proper development of neuronal tissue, and scaffolds capable of regulating this balance are essential for effective neuroregenerative strategies. Among the promising materials explored, AGMA1-based hydrogels have demonstrated particularly favorable biological properties. Indeed, existing literature regarding in vivo studies on AGMA1 hydrogel demonstrated therapeutic potential in a rat model with a transected sciatic nerve by supporting nerve regeneration [12]. However, their direct application is limited by their inherent softness, which compromises structural stability, an essential requirement for maintaining consistent conditions in in vitro studies, which are fundamental for investigating biological properties in terms of molecular mechanisms. To address this limitation, in the present study, AGMA1 hydrogels were reinforced with electrospun PLLA mats to develop a composite hydrogel, referred to as PLLA/H-AGMA20. This novel strategy aims to enhance mechanical strength while preserving biocompatibility. Electrospun PLLA mats are well-established for their biocompatibility and effectiveness in in vitro models, particularly for studying mechanisms underlying neurodegenerative diseases. Functionalization of PLLA fibers with novel chemical components such as bioactive hydrogel (H-AGMA20) has been shown to significantly enhance their ability to guide cell adhesion, and differentiation, and neuroprotection, thereby making them effective tools for neural tissue engineering. Furthermore, the development of scaffold-based hydrogel systems is crucial, providing a more robust and reliable platform for studying neuronal development and regeneration in three-dimensional (3D) environments. By providing both the mechanical support and biochemical cues necessary for neuronal differentiation, scaffolds such as PLLA/H-AGMA20 composites offer a promising platform for advancing therapies aimed at neural tissue regeneration and repair. To better contextualize the advantages of the PLLA/H-AGMA20 composite, it is important to consider its performance relative to commonly used biomaterials in neuroregeneration. While collagen scaffolds are widely appreciated for their biocompatibility and ability to support neural cell adhesion and growth [39], their rapid degradation and low mechanical strength limit their use in applications requiring sustained support. PLGA, a biodegradable and FDA-approved polymer, offers better mechanical properties and tunable degradation rates, but its acidic degradation by-products may induce inflammation, which is detrimental in neuroregenerative environments [40]. Chitosan has shown promise due to its bioactivity and ability to support nerve regeneration, yet its solubility challenges and mechanical limitations restrict its versatility [41,42]. PLLA alone, although mechanically robust and well suited for nanofiber fabrication via electrospinning, has minimal influence on neuroregenerative or neuroprotective responses due to its bioinert nature. In contrast, the PLLA/H-AGMA20 composite uniquely combines mechanical stability with biological functionality. Concerning our qualitative and quantitative analyses of preneuronal cell adhesion at 24 h, along with viability assessment from 1 to 14 days, the results revealed that although SH-SY5Y cell viability was initially lower on PLLA/H-AGMA$_{20}$ compared to the controls (tissue culture surface and PLLA) at day 1, it progressively increased over time. This suggests that the composite material is non-cytotoxic and supports cell adhesion and survival (Fig. 4A and B). Moreover, as the culture period extended, PLLA/H-AGMA$_{20}$ not only promoted neuronal differentiation but also effectively modulated the increase in cell number. These findings highlight the potential of the composite to promote neuronal growth and differentiation while regulating cell proliferation, making it a promising material for neuroregenerative applications. Fluorescence analysis (Fig. 4C) showed that PLLA/H-AGMA$_{20}$ induced a peak in GAP-43 expression, a marker of neuron maturation, in SH-SY5Y cells after 7 days of cell culture, compared to cells seeded on the tissue culture plate and on neat PLLA fibers used as controls. This increased expression of GAP-43 was sustained, with significantly high levels also observed after 14 days of culture. The qualitative findings on GAP-43 expression were further confirmed by image analysis (Fig. 4D) and confocal analysis (Fig. S10). Particularly, no GAP-43 expression was detected in SH-SY5Y cells grown on neat PLLA fibers, as shown in Fig. 4C and consistent with previous studies [25,26], highlighting the key role of the H-AGMA$_{20}$ hydrogel in promoting neuronal differentiation. These results are aligned with the excellent performance of the linear analogue of H-AGMA$_{20}$, which also demonstrated strong in vitro adhesion and proliferation capabilities on primary brain cells, including hippocampal neurons and astrocytes [16]. Furthermore, H-AGMA20 hydrogel compared to previous bioactive molecules used for PLLA functionalization [23,25,26] forms a surface at the interface with the cells useful not only for producing

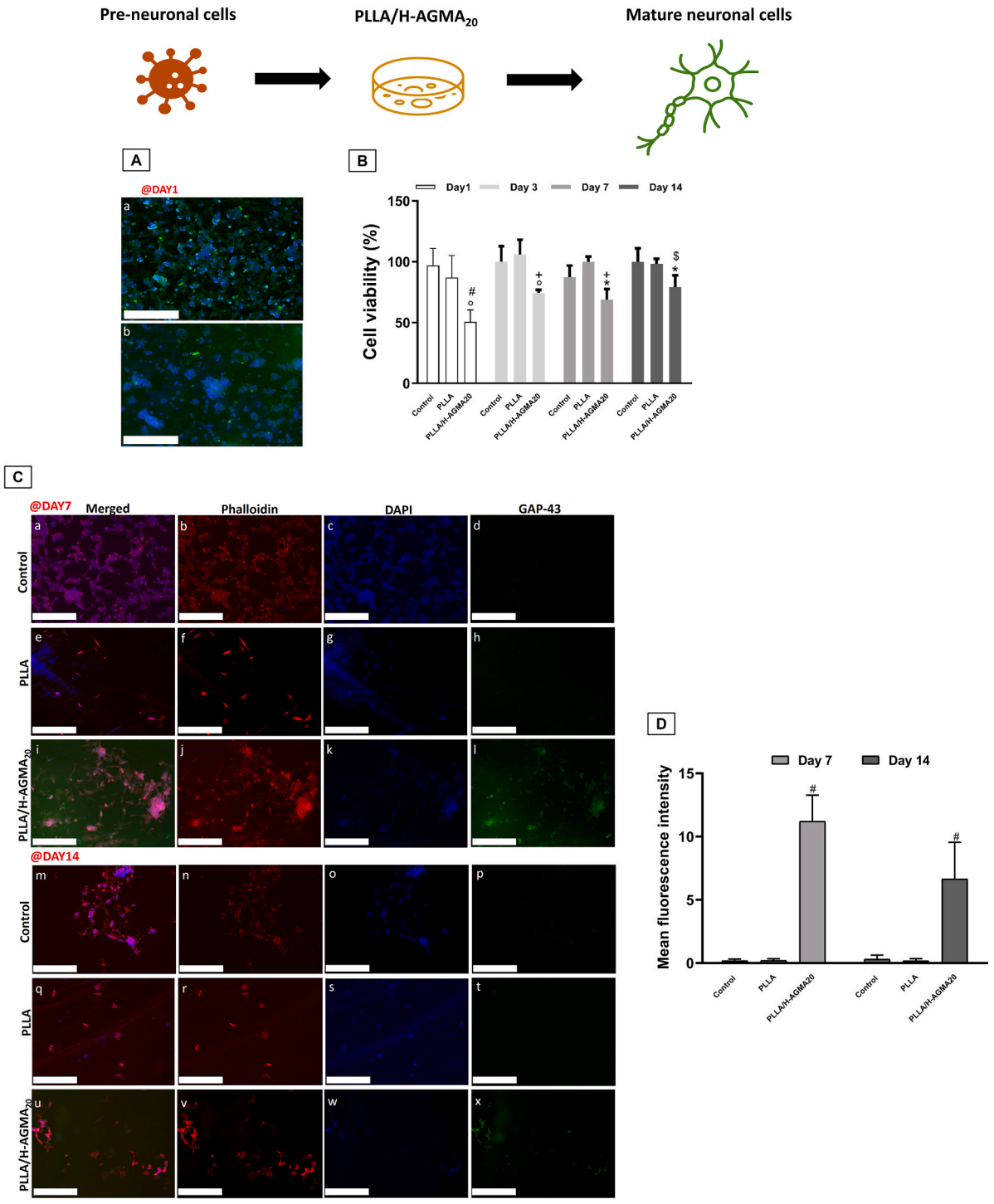

Fig. 4. Effect of PLLA/H-AGMA$_{20}$ on SH-SY5Y cell adhesion, viability and differentiation marker (GAP-43). Qualitative SH-SY5Y cell adhesion after 24 h of cell culture was tested through fluorescence analysis in the absence (a) and in the presence (b) of PLLA/H-AGMA$_{20}$ (merged images of FITC-Phalloidin for cytoskeleton in green and DAPI staining for nuclei in blue), Magnification 10× Scale bar: 125 μm (A). Cell viability was assessed using the AlamarBlue® assay (B). Lower cell viability was observed on day 1 for PLLA/H-AGMA$_{20}$ compared to the control; however, this effect disappeared by day 7, where the material regulated the increase in cell number over the culture period, maintaining its influence up to 14 days of exposure ($^{*}p \leq 0.05$ and $^{\circ}p \leq 0.001$ vs Control; $^{\$}$p 0,05, $^{+}$p 0,001 and $^{\#}$p 0,0001vs PLLA). Fluorescence analysis on cell differentiation was performed using the GAP-43 marker expression. Upon fixation cells were stained with specific antibodies: Anti-GAP-43 (in green) and anti- Phalloidin-ATTO 594 (F-actin, in red) staining; nuclei were detected by DAPI (in blue) staining (a,e,i,m,q,u = merged; b,f,j,n,r,v = cytoskeleton; c,g,k,o,s,w = nuclei; d,h,l,p,t,x = GAP-43). Magnification 10× Scale bar: 250 μm (C). Image analysis of GAP-43 expression ($^{\#}p \leq 0.0001$ vs Controls;). The fluorescence intensity was normalized to the number of cells per surface. Results are mean ± SD and the images are representative of 3 independent experiments (D). (For interpretation of the references to color in this figure legend, the reader is referred to the web version of this article.)

neuroregenerative and neuroprotective chemical signals, but also for better mimicking the extracellular matrix, thus improving the biological response.

3.4.2. *In vitro evaluation of PLLA/H-AGMA$_{20}$ on SH-SY5Y cell response to MPP$^+$ stimulation*

To study the neuroprotective properties of PLLA/H-AGMA$_{20}$, SH-SY5Y cells, differentiated for 7 days on PLLA/H-AGMA$_{20}$ samples, were exposed to the MPP$^+$ neurotoxin for 24 h. Cell viability analysis

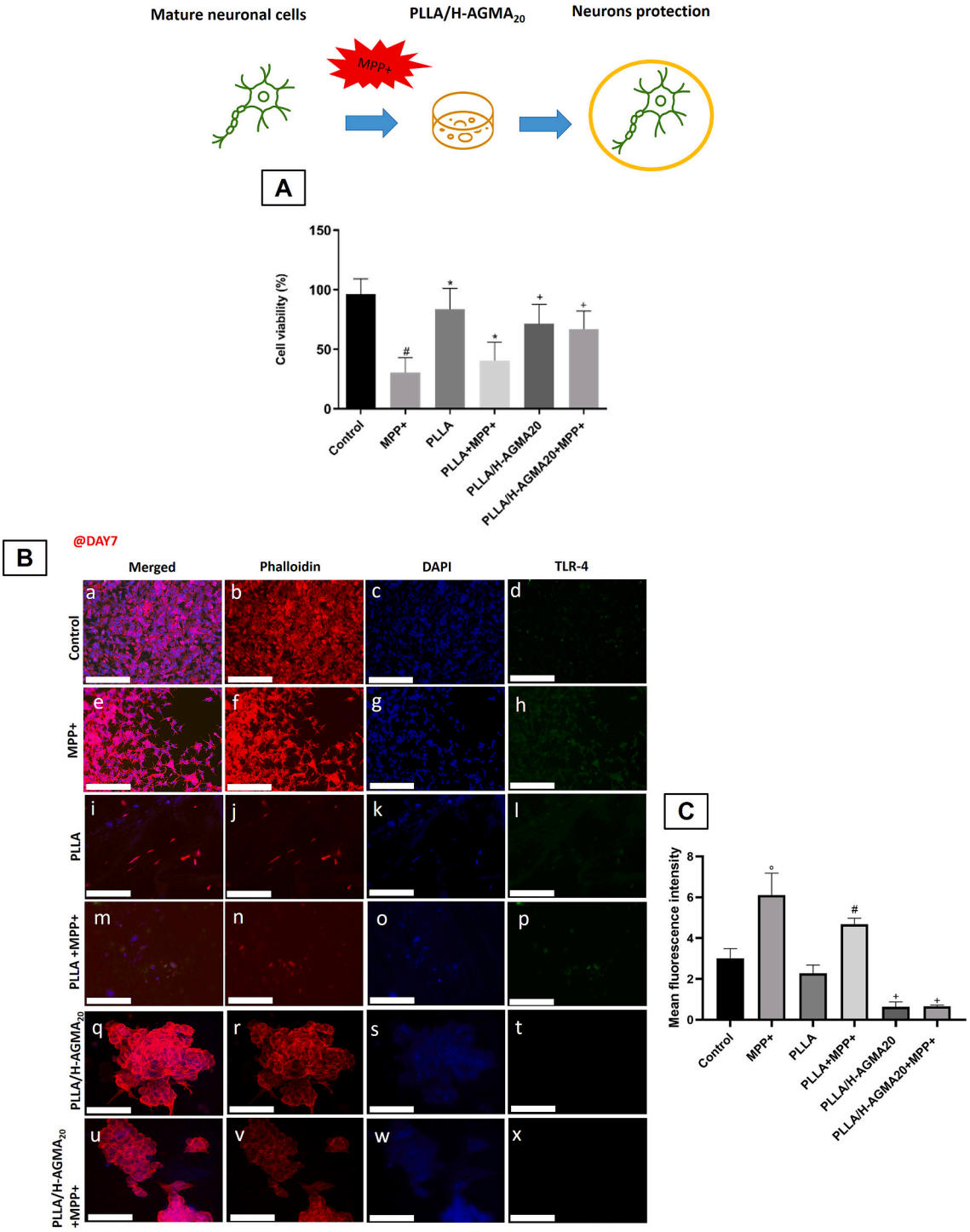

Fig. 5. Effect of PLLA/H-AGMA$_{20}$ on in vitro MPP+ stimulation of SH-SY5Y cells. Cell viability evaluated using the AlamarBlue® assay. PLLA/H-AGMA$_{20}$ inhibited MPP+ cytotoxic effect on SH-SY5Y cells after 7 days of cell culture and 24 h MPP+ exposure ($^*p \leq 0.05$ and $^{\#}p \leq 0.0001$ vs Control; $^{+}p \leq 0.0001$ vs MPP+); (A). Fluorescence analysis on TLR-4 expression was performed after cell fixation and staining with specific antibodies on day 7 of cell culture and after 24 h MPP+ exposure: anti-TLR-4 (in green) and anti-Phalloidin-ATTO 594 (F-actin, in red) staining; nuclei were detected by DAPI (in blue) staining, (a,e,i,m,q,u = merged; b,f,j, n,r,v = cytoskeleton; c,g,k,o,s,w = nuclei; d,h,l,p,t,x = TLR-4). Magnification 10×. Scale bar: 250 μm. Results are mean ± SD and are representative of 3 independent experiments (B). Image analysis of TLR-4 expression ($^{\circ}p \leq 0.001$ vs Control; #p ≤ 0.0001 vs PLLA and + p ≤ 0.001 vs PLLA+MPP$^+$). The fluorescence intensity was normalized to the number of cells per surface. Results are mean ± SD and the images are representative of 3 independent experiments (C). (For interpretation of the references to color in this figure legend, the reader is referred to the web version of this article.)

showed that MPP^+ significantly reduced cell survival on both the tissue culture plate and neat PLLA fibers used as controls (Fig. 5A). In contrast, no significant changes in SH-SY5Y cell survival were observed in cells grown on PLLA/H-AGMA$_{20}$ in the presence of MPP^+, compared to those grown on PLLA/H-AGMA$_{20}$ without MPP^+ stimulation. This suggests that PLLA/H-AGMA$_{20}$ exerts a neuroprotective effect against MPP^+-induced toxicity (Fig. 5A). It was established that MPP^+ induces TLR-4 overexpression in SH-SY5Y cells [43]. Here, biological studies have confirmed this finding, demonstrating that MPP^+ stimulation led to upregulation of TLR-4 expression in SH-SY5Y cells compared to basal levels [44]. Notably, PLLA/H-AGMA$_{20}$ was also able to inhibit both basal (tissue culture plate and PLLA controls) and MPP^+ induced TLR-4 expression after 7 days of cell culture and 24 h of MPP^+ exposure (Fig. 5B). The qualitative data on TLR-4 expression were further confirmed by image analysis, as shown in Fig. 5C. These results suggest that PLLA/H-AGMA$_{20}$ not only supports cell viability but also mitigates inflammatory pathways associated with neurotoxin exposure, thus enhancing its potential as a neuroprotective biomaterial in neurodegenerative disease models.

3.4.3. *In vitro effect of PLLA/H-AGMA20 on the inflammatory response*

It has been previously reported that LPS selectively activates TLR-4 cascade in microglia, the resident macrophages of the central nervous system (CNS), leading to the secretion of inflammatory markers. Additionally, eumelanin-decorated PLLA has been shown to influence this pathway by downregulating its expression and inhibiting basal levels in cells not treated with LPS [26]. Furthermore, an upregulated inflammatory response in the CNS determines proinflammatory cytokines, including IL-1β, and nitric oxide (NO), which are crucial in the induction of neuroinflammation and the regulation of redox balance, ultimately leading to neuronal tissue injury [26]. Thus, we aimed to investigate the potential antinflammatory properties of PLLA/H-AGMA$_{20}$ in both SH-SY5Y cells stimulated with MPP^+ and immune-responsive RAW 264.7 macrophages stimulated with LPS. While PLLA has been explored in previous studies, it was not evaluated in this experiment due to its limited ability to modulate the inflammatory response on its own [26]. In contrast, the PLLA/H-AGMA$_{20}$ composite was chosen for its enhanced properties, particularly its ability to regulate inflammatory markers more effectively.

The results from SH-SY5Y cells stimulated with MPP^+ showed a significant increase in nitrite levels and IL-1β production. However, when SH-SY5Y cells were grown on PLLA/H-AGMA20, both nitrite and IL-1β levels were significantly reduced (Fig. 6a and b), suggesting a strong anti-inflammatory effect. Interestingly, MPP^+ alone induced an anti-inflammatory response, as evidenced by IL-10 production, with no significant differences observed in the presence of PLLA/H-AGMA20

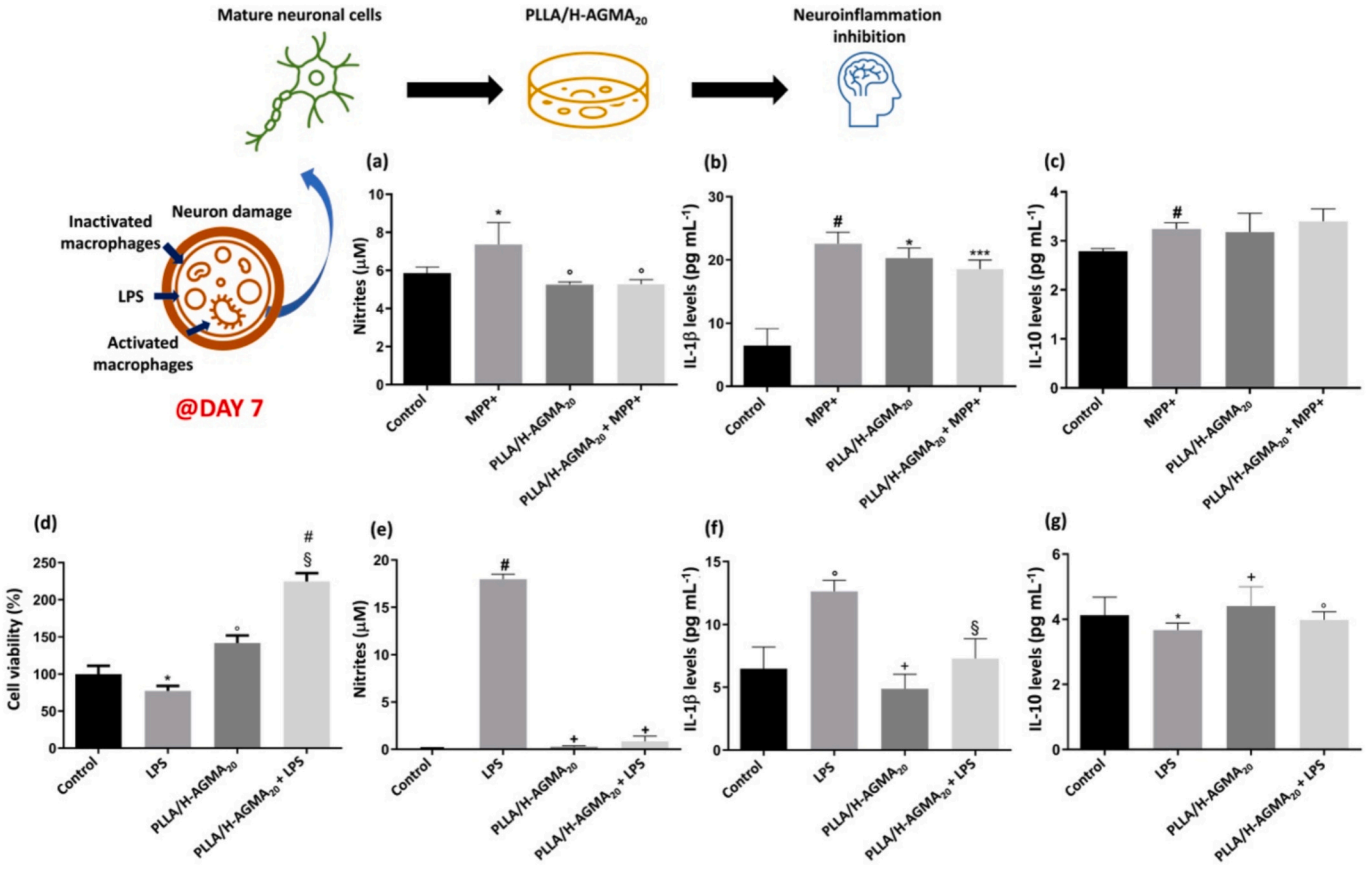

Fig. 6. Effect of PLLA/H-AGMA$_{20}$ on SH-SY5Y and RAW 264.7 in vitro inflammatory response. The exposure of SH-SY5Y cells to MPP^+ and of RAW 264.7 cells to LPS (24 h) after 7 days of cell culture significantly increases nitrite production compared to control, while PLLA/H-AGMA$_{20}$ induces a reduction in nitrite production ($^*p \leq 0.05$ and $^{\#}p \leq 0.0001$ vs Control; $^{\circ}p \leq 0.001$ vs MPP^+ and $^{+}p \leq 0.0001$ vs LPS (a and e). Effect of PLLA/H-AGMA$_{20}$ on IL-1β levels in SH-SY5Y cells and RAW 264.7 cells exposed to MPP^+ and LPS, respectively, for 24 h; IL-1β levels significantly decrease in the presence of PLLA/H-AGMA$_{20}$ compared to MPP^+ ($^*p \leq 0.05$ and $^{***}p \leq 0.0001$ vs MPP+) and LPS ($^{\S}p \leq 0.001$ and $+ p \leq 0.0001$ vs LPS) alone that significantly increased IL-1β levels ($^{\circ}p \leq 0.001$ and $^{\#}p \leq 0.0001$ vs Control) (b and f). RAW 264.7 cell viability was evaluated using the AlamarBlue® assay (d). PLLA/H-AGMA$_{20}$ significantly improves RAW 264.7 cell viability after 7 days cell culture and 24 h LPS exposure ($^*p \leq 0.05$; $^{\circ}p \leq 0.001$ vs Control; $^{\S}p \leq 0.001$ vs PLLA/H-AGMA$_{20}$ and $^{\#}p \leq 0.0001$ vs LPS). Effect of PLLA/H-AGMA$_{20}$ on IL-10 levels in SH-SY5Y cells and RAW 264.7 cells exposed to MPP+ and LPS, respectively, for 24 h; IL-10 levels significantly increase ($^{\#}p \leq 0.0001$ vs Control) in the presence of MPP^+ alone. No differences were observed after PLLA/H-AGMA$_{20}$ exposure (c and g). LPS induced a significant decrease in IL-10 production reverted by PLLA/H-AGMA$_{20}$ exposure ($^{\circ}p \leq 0.001$ and $^{+}p \leq 0.0001$ vs LPS). Results are mean ± SD of 3 independent experiments.

(Fig. 6c).

A more evident effect of PLLA/H-AGMA$_{20}$ was observed in RAW 264.7 macrophages following LPS stimulation. The biocompatibility of PLLA/H-AGMA$_{20}$ with RAW 264.7 macrophages was first evaluated in terms of cell viability. As shown in Fig. 6d, PLLA/H-AGMA$_{20}$ promoted cell survival on day 7 of culture, even after 24 h of LPS exposure. Specifically, PLLA/H-AGMA20 significantly decreased the levels of nitrite and IL-1β, both of which were elevated by LPS stimulation (Fig. 6e and f). Additionally, PLLA/H-AGMA20 significantly increased IL-10 levels, which were otherwise suppressed by LPS treatment (Fig. 6g). These findings show that PLLA/H-AGMA20 not only supports cell survival but also modulates the inflammatory response, further demonstrating its potential as a neuroprotective and anti-inflammatory agent.

3.4.4. *Mechanism of action of the PLLA/H-AGMA20 composite hydrogel*

In order to deepen how PLLA/H-AGMA20 exerts its neuroprotective and neuroregenerative effects, potential molecular pathways modulated by the composite hydrogel have been explored. Specifically, inflammatory signaling cascades such as Caspase-1 and neurotrophic factors (β-NGF) have been quantified using fluorescence analysis. According to previous studies, the caspase family has been recognized as a key contributor to neuronal cell death, thereby playing a critical role in the progression of neuronal degeneration [45]. Caspase-1 is a component of NLRP3 (NOD-like receptor pyrin domain containing 3) inflammasome complex and plays a key role in neuroinflammation by activating microglia [45].

Furthermore, it has been demonstrated that MPP$^+$ stimulation in SH-SY5Y cells induces caspase-1 activation, followed by Caspase-7 cleavage, nuclear translocation of poly (ADPribose) polymerase 1 (PARP1), and increased release of apoptosis-inducing factor (AIF).

Here, we showed that PLLA/H-AGMA20 significantly inhibited Caspase-1 expression in SH-SY5Y cells following MPP$^+$ stimulation after 7 days of cell-material interaction (Fig. 7A). This effect was accompanied by protection against apoptosis through caspase-7/PARP1/AIF pathway (Fig. 7B), confirming the neuroprotective effect of PLLA/H-AGMA20 against MPP + -induced toxicity.

Notably, PLLA alone did not reduce MPP$^+$-induced caspase-1 expression, suggesting that the neuroprotective signal is primarily attributable to the hydrogel component. The qualitative data on caspase-1 expression were further confirmed by image analysis, as shown in Fig. 7C. In addition, we found that PLLA/H-AGMA20 maintained high levels of β-NGF in SH-SY5Y cells (Fig. S11), that plays a crucial role in neuronal survival and differentiation [46]. Hence, the presence of H-AGMA20 in our composite not only improves cell adhesion and differentiation but also contributes to the modulation of inflammatory signaling pathways, such as the Caspase-1 cascade, and enhances

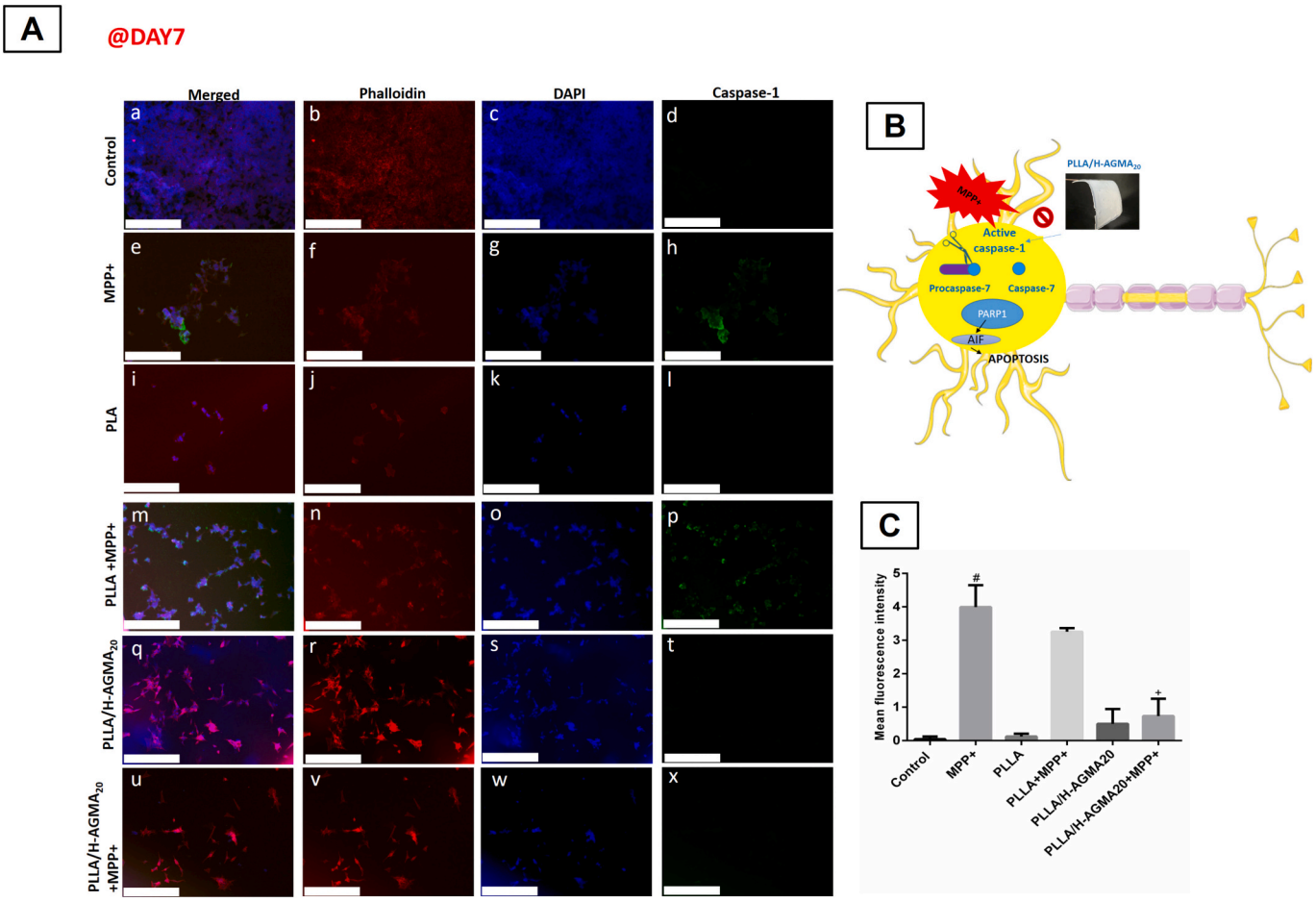

Fig. 7. Effect of PLLA/H-AGMA20 on in vitro MPP$^+$-induced Caspase-1 expression. Fluorescence analysis on Caspase-1 expression was performed after cell fixation and staining with specific antibodies on day 7 of cell culture and after 24 h MPP$^+$ exposure: anti-Caspase-1 (in green) and anti-Phalloidin-ATTO 594 (F-actin, in red) staining; nuclei were detected by DAPI (in blue) staining, (a,e,i,m,q,u = merged; b,f,j,n,r,v = cytoskeleton; c,g,k,o,s,w = nuclei; d,h,l,p,t,x = Caspase-1). Magnification 10×. Scale bar: 250 μm. Results are mean ± SD and are representative of 3 independent experiments (A). Schematic representation for the inhibitory effect of PLLA/H-AGMA20 on Caspase-1 pathway: MPP$^+$ activates caspase-1 that cleaves pro-caspase-7 into caspase7. Subsequently, caspase-7 induces nuclear translocation of PARP1 and AIF release in the cytoplasm, leading to neuron apoptosis. Image analysis of Caspase-1 expression ($\#p \leq 0.0001$ vs Control and $^{+}p \leq 0.0001$ vs PLLA+MPP$^+$). The fluorescence intensity was normalized to the number of cells per surface. Results are mean ± SD and the images are representative of 3 independent experiments (C). (For interpretation of the references to color in this figure legend, the reader is referred to the web version of this article.)

neurotrophic factor (β-NGF) production. These results indicate that the composite not only maintains structural integrity over time but also actively supports a regenerative and neuroprotective cellular environment an advantage over many existing single-component biomaterials. This dual functionality positions the PLLA/H-AGMA20 system as a strong candidate for advanced neuroregenerative strategies.

4. Conclusions

In this study, a 490 μm thick PLLA/H-$AGMA_{20}$ composite hydrogel was successfully obtained by impregnating a 100 μm thick electrospun PLLA mat - surface modified with amine groups via a facile aminolysis reaction—with an aqueous solution of the α,ω-acrylamide-terminated $AGMA_{20}$ oligomer, a biocompatible cell-adhesive polyamidoamine, and curing it through UV-induced radical polymerization of the acrylamide terminals. PLLA/$AGMA_{20}$ absorbed amounts of water comparable to those of the virgin H-$AGMA_{20}$ hydrogel and, in its hydrated state, remained soft and pliable. In fact, the presence of the reinforcing layer affects the mechanical behavior leading to very high toughness for the PLLA/$AGMA_{20}$ respect to the neat hydrogel, even if lower than that of the neat PLLA fibers because the fiber stretching ability under stress were restricted by the interconnections with the hydrogel matrix.

Notably, PLLA/$AGMA_{20}$ effectively promoted SH-SY5Y neuronal cell growth and maturation in vitro, without the need for differentiation factors in the culture medium. Moreover, it showed significant neuroprotective properties by defending SH-SY5Y cells from MPP^+ induced neurotoxicity. PLLA/$AGMA_{20}$ also exhibited the ability to mitigate neurodegeneration-related neuroinflammation, modulating the inflammatory response in both pre-neuronal and macrophages cell lines. Overall, these promising properties position PLLA/$AGMA_{20}$ as an attractive candidate to be further explored in in vitro models of neurodegenerative conditions characterized by neuronal damage and inflammation.

Abbreviations

PLLA	Poly-L-lactic acid
PAA	Polyamidoamine
H-$AGMA_{20}$	Polyamidoamine-based hydrogel
PBS	Phosphate Buffered Saline
LPS	lipopolysaccharide
MPP +	1-methyl-4-phenylpyridinium iodide
EDA	ethylenediamine
BAC	2,2′-bis(acrylamido)acetic acid
NMR	nuclear magnetic resonance spectrometry.
FT-IR/ATR	Fourier transform-infrared spectroscopy in attenuated total reflectance
FE-SEM	Field-emission scanning electron microscope
XRD	X-ray diffraction
TGA	Thermogravimetric analysis
SH-SY5Y cells	Neuroblastoma cell line derived from a metastatic bone tumor from a 4-year-old cancer patient
RAW 264.7 cells	Macrophage cell line from a male mouse
DMEM	Dulbecco's modified Eagle medium
FITC	Fluorescein 5(6)-isothiocyanate
GAP-43	Growth associated protein 43
DAPI	4′,6-Diamidino-2-phenylindole
TLR	Toll-like receptors
β-NGF	beta nerve growth factor
NLRP3	NLR family pyrin domain containing 3
PARP1	poly(ADP-ribose) polymerase 1
AIF	apoptosis-inducing factor

CRediT authorship contribution statement

Sofia Treccani: Investigation, Data curation. **Irene Bonadies:** Writing – review & editing, Writing – original draft, Methodology. **Paolo Ferruti:** Conceptualization. **Jenny Alongi:** Writing – review & editing. **Enrico Scarpa:** Methodology, Investigation. **Paola Laurienzo:** Writing – review & editing, Supervision, Conceptualization. **Maria Grazia Raucci:** Writing – review & editing, Supervision, Methodology, Funding acquisition. **Ines Fasolino:** Writing – review & editing, Writing – original draft, Methodology, Investigation, Funding acquisition, Data curation, Conceptualization. **Elisabetta Ranucci:** Writing – original draft, Supervision, Methodology, Conceptualization.

Declaration of Generative AI and AI-assisted technologies in the writing process

The authors did not use any form of AI for preparation of this paper.

Declaration of competing interest

The authors declare that they have no known competing financial interests or personal relationships that could have appeared to influence the work reported in this paper.

Acknowledgments

This work was funded by the European Union - Next Generation EU, Mission 4, Component 2, INVESTIMENTO 1.3 “CNR multidisciplinary advanced platform for targeting neuronal and glial homeostasis CNR-INVENIT". CUP E63C22002170007 [M.G. Raucci] and by European Union - Next Generation EU, Mission 4, Component 2, INVESTIMENTO 1.1 "INFLAMM-ALS”, PRIN2022 2022BNZLMN - CUP B53D23018520006 [I. Fasolino].

The Authors thank I. Campostrini and Unitech NOLIMITS platform, and S. Vitali (Università degli Studi di Milano) for the SEM observations and XRD experiments, respectively. The authors also thank Mariarosaria Bonetti for lab technical support, Dr. Roberta Marzella for supporting project management and https://smart.servier.com/ website for graphical abstract realization.

Appendix A. Supplementary data

^{1}H NMR spectrum of BAC in DMSO-d_6. ^{1}H NMR spectrum of the $AGMA_{20}$ oligomer in D_2O. PLLA/H-$AGMA_{20}$ preparation steps. Optical micrographs of a fully hydrated H-$AGMA_{20}$ hydrogel. Optical micrographs of water-swollen PLLA/H-$AGMA_{20}$ composites prepared from EDA-treated PLLA. Water absorption ability of PLLA/H-$AGMA_{20}$ and H-$AGMA_{20}$. Reversible water uptake in absorbing/drying cycles. FT-IR/ATR spectra of PLLA mat, H-$AGMA_{20}$ and PLLA/H-$AGMA_{20}$. Representative stress-strain curves of PLLA/H-$AGMA_{20}$ and PLLA. Confocal analysis on cell differentiation through GAP-43 marker expression. Supplementary data to this article can be found online at https://doi.org/10.1016/j.bioadv.2025.214415.

Data availability

The authors declare that all data supporting the findings of this study are available within the paper; source data for the figures in this study are available from the authors upon request.

References

[1] A. Slanzi, G. Iannoto, B. Rossi, E. Zenaro, G. Constantin, In vitro models of neurodegenerative diseases, Front. Cell Dev. Biol. 8 (2020) 328, https://doi.org/10.3389/fcell.2020.00328.

[2] P.A. Walczak, P. Perez-Esteban, D.C. Bassett, E.J. Hill, Modelling the central nervous system: tissue engineering of the cellular microenvironment, Emerging Topics in Life Sciences 5 (2021) 507–517, https://doi.org/10.1042/ETLS20210245.

[3] M. Razavi (Ed.), Biomaterials for Tissue Engineering, Bentham Science Publishers, Sharjah, 2017.

[4] S. Mantha, S. Pillai, P. Khayambashi, A. Upadhyay, Y. Zhang, O. Tao, H.M. Pham, S.D. Tran, Smart hydrogels in tissue engineering and regenerative medicine, Materials 12 (2019) 3323, https://doi.org/10.3390/ma12203323.

[5] E. Martí Coma-Cros, A. Biosca, J. Marques, L. Carol, P. Urbán, D. Berenguer, M. C. Riera, M. Delves, R.E. Sinden, J.J. Valle-Delgado, L. Spanos, I. Siden-Kiamos, P. Pérez, K. Paaijmans, M. Rottmann, A. Manfredi, P. Ferruti, E. Ranucci, X. Fernàndez-Busquets, Polyamidoamine nanoparticles for the oral administration of antimalarial drugs, Pharmaceutics 10 (2018) 225, https://doi.org/10.3390/pharmaceutics10040225.

[6] E. Ranucci, A. Manfredi, Polyamidoamines: versatile bioactive polymers with potential for biotechnological applications, Chem. Afr. 2 (2019) 167–193, https://doi.org/10.1007/s42250-019-00046-1.

[7] M. Donalisio, E. Ranucci, V. Cagno, A. Civra, A. Manfredi, R. Cavalli, P. Ferruti, D. Lembo, Agmatine-containing poly(amidoamine)s as a novel class of antiviral macromolecules: structural properties and *in vitro* evaluation of infectivity inhibition, Antimicrob. Agents Chemother. 58 (2014) 6315–6319, https://doi.org/10.1128/AAC.03420-14.

[8] E. Jacchetti, E. Emilitri, S. Rodighiero, M. Indrieri, A. Gianfelice, C. Lenardi, A. Podestà, E. Ranucci, P. Ferruti, P. Milani, Biomimetic poly(amidoamine) hydrogels as synthetic materials for cell culture, J Nanobiotechnol 6 (2008) 14, https://doi.org/10.1186/1477-3155-6-14.

[9] P. Ferruti, S. Bianchi, E. Ranucci, F. Chiellini, A.M. Piras, Novel Agmatine-containing poly(amidoamine) hydrogels as scaffolds for tissue engineering, Biomacromolecules 6 (2005) 2229–2235, https://doi.org/10.1021/bm050210+.

[10] G. Dos Reis, F. Fenili, A. Gianfelice, G. Bongiorno, D. Marchesi, P.E. Scopelliti, A. Borgonovo, A. Podestà, M. Indrieri, E. Ranucci, P. Ferruti, C. Lenardi, P. Milani, Direct microfabrication of topographical and chemical cues for the guided growth of neural cell networks on Polyamidoamine hydrogels, Macromol. Biosci. 10 (2010) 842–852, https://doi.org/10.1002/mabi.200900410.

[11] N. Mauro, A. Manfredi, E. Ranucci, P. Procacci, M. Laus, D. Antonioli, C. Mantovani, V. Magnaghi, P. Ferruti, Degradable poly(amidoamine) hydrogels as scaffolds for in vitro culturing of peripheral nervous system cells, Macromol. Biosci. 13 (2013) 332–347, https://doi.org/10.1002/mabi.201200354.

[12] V. Magnaghi, V. Conte, P. Procacci, G. Pivato, P. Cortese, E. Cavalli, G. Pajardi, E. Ranucci, F. Fenili, A. Manfredi, P. Ferruti, Biological performance of a novel biodegradable polyamidoamine hydrogel as guide for peripheral nerve regeneration, J. Biomed. Mater. Res. 98A (2011) 19–30, https://doi.org/10.1002/jbm.a.33091.

[13] J. Franchini, E. Ranucci, P. Ferruti, M. Rossi, R. Cavalli, Synthesis, physicochemical properties, and preliminary biological characterizations of a novel amphoteric Agmatine-based poly(amidoamine) with RGD-like repeating units, Biomacromolecules 7 (2006) 1215–1222, https://doi.org/10.1021/bm060054m.

[14] R. Cavalli, A. Bisazza, R. Sessa, L. Primo, F. Fenili, A. Manfredi, E. Ranucci, P. Ferruti, Amphoteric Agmatine containing Polyamidoamines as carriers for plasmid DNA in vitro and in vivo delivery, Biomacromolecules 11 (2010) 2667–2674, https://doi.org/10.1021/bm100685t.

[15] M. Donalisio, P. Quaranta, F. Chiuppesi, M. Pistello, V. Cagno, R. Cavalli, M. Volante, A. Bugatti, M. Rusnati, E. Ranucci, P. Ferruti, D. Lembo, The AGMA1 poly(amidoamine) inhibits the infectivity of herpes simplex virus in cell lines, in human cervicovaginal histocultures, and in vaginally infected mice, Biomaterials 85 (2016) 40–53, https://doi.org/10.1016/j.biomaterials.2016.01.055.

[16] N. Tonna, F. Bianco, M. Matteoli, C. Cagnoli, F. Antonucci, A. Manfredi, N. Mauro, E. Ranucci, P. Ferruti, A soluble biocompatible guanidine-containing polyamidoamine as promoter of primary brain cell adhesion and *in vitro* cell culturing, Sci. Technol. Adv. Mater. 15 (2014) 045007, https://doi.org/10.1088/1468-6996/15/4/045007.

[17] M.O. Teixeira, J.C. Antunes, H.P. Felgueiras, Recent advances in fiber–hydrogel composites for wound healing and drug delivery systems, Antibiotics 10 (2021) 248, https://doi.org/10.3390/antibiotics10030248.

[18] J. Li, L. Gao, R. Xu, S. Ma, Z. Ma, Y. Liu, Y. Wu, L. Feng, M. Cai, F. Zhou, Fibers reinforced composite hydrogels with improved lubrication and load-bearing capacity, Friction 10 (2022) 54–67, https://doi.org/10.1007/s40544-020-0389-9.

[19] S. Xu, L. Deng, J. Zhang, L. Yin, A. Dong, Composites of electrospun-fibers and hydrogels: a potential solution to current challenges in biological and biomedical field, J. Biomed. Mater. Res. 104 (2016) 640–656, https://doi.org/10.1002/jbm.b.33420.

[20] C. Gualandi, N. Bloise, N. Mauro, P. Ferruti, A. Manfredi, M. Sampaolesi, A. Liguori, R. Laurita, M. Gherardi, V. Colombo, L. Visai, M.L. Focarete, E. Ranucci, Poly- l -lactic acid nanofiber–polyamidoamine hydrogel composites: preparation, properties, and preliminary evaluation as scaffolds for human pluripotent stem cell culturing, Macromol. Biosci. 16 (2016) 1533–1544, https://doi.org/10.1002/mabi.201600061.

[21] F. Maggi, A. Manfredi, F. Carosio, L. Maddalena, J. Alongi, P. Ferruti, E. Ranucci, Toughening Polyamidoamine hydrogels through covalent grafting of short silk fibers, Molecules 27 (2022) 7808, https://doi.org/10.3390/molecules27227808.

[22] P. Ferruti, J. Alongi, E. Barabani, A. Manfredi, E. Ranucci, Silk/polyamidoamine membranes for removing chromium VI from water, Polymers 15 (2023) 1871, https://doi.org/10.3390/polym15081871.

[23] A. Mariano, I. Fasolino, N.B. Dinger, C. Latte Bovio, I. Bonadies, A. Pezzella, L. Ambrosio, M.G. Raucci, F. Santoro, Eumelanin-coated aligned PLA electrospun microfibers to guide SH-SY5Y cells spreading, alignment, and maturation, Adv Materials Inter 10 (2023) 2202022, https://doi.org/10.1002/admi.202202022.

[24] V.A. Baldassarro, L.S. Dolci, C. Mangano, L. Giardino, C. Gualandi, M.L. Focarete, L. Calzà, *In vitro* testing of biomaterials for neural repair: focus on cellular systems and high-content analysis, Biores. Open Access 5 (2016) 201–211, https://doi.org/10.1089/biores.2016.0025.

[25] I. Fasolino, I. Bonadies, L. Ambrosio, M.G. Raucci, C. Carfagna, F.M. Caso, F. Cimino, A. Pezzella, Eumelanin coated PLA electrospun Micro fibers as bioinspired cradle for SH-SY5Y neuroblastoma cells growth and maturation, ACS Appl. Mater. Interfaces 9 (2017) 40070–40076, https://doi.org/10.1021/acsami.7b13257.

[26] I. Fasolino, E.D. Carvalho, M.G. Raucci, I. Bonadies, A. Soriente, A. Pezzella, A. P. Pêgo, L. Ambrosio, Eumelanin decorated poly(lactic acid) electrospun substrates as a new strategy for spinal cord injury treatment, Biomaterials Advances 146 (2023) 213312, https://doi.org/10.1016/j.bioadv.2023.213312.

[27] Y.J. Park, D.M. Yu, J.H. Ahn, J.-H. Choi, Y.T. Hong, Surface modification of polyimide films by an ethylenediamine treatment for a flexible copper clad laminate, Macromol. Res. 20 (2012) 168–173, https://doi.org/10.1007/s13233-012-0025-2.

[28] T. Haddad, S. Noel, B. Liberelle, R. El Ayoubi, A. Ajji, G. De Crescenzo, Fabrication and surface modification of poly lactic acid (PLA) scaffolds with epidermal growth factor for neural tissue engineering, Biomatter 6 (2016) e1231276, https://doi.org/10.1080/21592535.2016.1231276.

[29] A. Walzl, C. Unger, N. Kramer, D. Unterleuthner, M. Scherzer, M. Hengstschläger, D. Schwanzer-Pfeiffer, H. Dolznig, The Resazurin reduction assay can distinguish cytotoxic from cytostatic compounds in spheroid screening assays, SLAS Discovery 19 (2014) 1047–1059, https://doi.org/10.1177/1087057114532352.

[30] P. Zhou, R. Weng, Z. Chen, R. Wang, J. Zou, X. Liu, J. Liao, Y. Wang, Y. Xia, Q. Wang, TLR4 signaling in MPP^{+} -induced activation of BV-2 cells, Neural Plast. 2016 (2016) 1–9, https://doi.org/10.1155/2016/5076740.

[31] G. Mallamaci, B. Brugnoli, A. Mariano, A.S. d'Abusco, A. Piozzi, V. Di Lisio, E. Sturabotti, S. Alfano, I. Francolini, Surface modification of polyester films with polyfunctional amines: effect on bacterial biofilm formation, Surf Interfaces 39 (2023) 102924, https://doi.org/10.1016/j.surfin.2023.102924.

[32] M. Friedman, Applications of the Ninhydrin reaction for analysis of amino acids, peptides, and proteins to agricultural and biomedical sciences, J. Agric. Food Chem. 52 (2004) 385–406, https://doi.org/10.1021/jf030490p.

[33] J. Yang, F. Li, G. Lu, Y. Lu, C. Song, R. Zhou, S. Wu, Electrospun biodegradable poly (L-lactic acid) nanofiber membranes as highly porous oil sorbent nanomaterials, Nanomaterials 12 (2022) 2670, https://doi.org/10.3390/nano12152670.

[34] B.K. Tarus, N. Fadel, A. Al-Oufy, M. El-Messiry, Investigation of mechanical properties of electrospun poly (vinyl chloride) polymer nanoengineered composite, J. Eng. Fibers Fabr. 15 (2020) 1558925020982569, https://doi.org/10.1177/1558925020982569.

[35] Z. Wu, Z. Zhang, W. Wei, Y. Yin, C. Huang, J. Ding, Q. Duan, Investigation of a novel poly (lactic acid) porous material toughened by thermoplastic polyurethane, J. Mater. Sci. 57 (2022) 5456–5466, https://doi.org/10.1007/s10853-022-06951-0.

[36] A. Manfredi, F. Carosio, P. Ferruti, E. Ranucci, J. Alongi, Linear polyamidoamines as novel biocompatible phosphorus-free surface-confined intumescent flame retardants for cotton fabrics, Polym. Degrad. Stab. 151 (2018) 52–64, https://doi.org/10.1016/j.polymdegradstab.2018.02.020.

[37] N.J. Fiore, J.D. Tamer-Mahoney, A. Beheshti, T.J.F. Nieland, D.L. Kaplan, 3D biocomposite culture enhances differentiation of dopamine-like neurons from SH-SY5Y cells: a model for studying Parkinson's disease phenotypes, Biomaterials 290 (2022) 121858, https://doi.org/10.1016/j.biomaterials.2022.121858.

[38] S. Ruijtenberg, S. Van Den Heuvel, Coordinating cell proliferation and differentiation: antagonism between cell cycle regulators and cell type-specific gene expression, Cell Cycle 15 (2016) 196–212, https://doi.org/10.1080/15384101.2015.1120925.

[39] X. Gu, F. Ding, D.F. Williams, Neural tissue engineering options for peripheral nerve regeneration, Biomaterials 35 (2014) 6143–6156, https://doi.org/10.1016/j.biomaterials.2014.04.064.

[40] R.A. Jain, The manufacturing techniques of various drug loaded biodegradable poly(lactide-co-glycolide) (PLGA) devices, Biomaterials 21 (2000) 2475–2490, https://doi.org/10.1016/S0142-9612(00)00115-0.

[41] T.F. Cova, B.F. Milne, A.A.C.C. Pais, Host flexibility and space filling in supramolecular complexation of cyclodextrins: a free-energy-oriented approach, Carbohydr. Polym. 205 (2019) 42–54, https://doi.org/10.1016/j.carbpol.2018.10.009.

[42] M. Dash, F. Chiellini, R.M. Ottenbrite, E. Chiellini, Chitosan—a versatile semi-synthetic polymer in biomedical applications, Prog. Polym. Sci. 36 (2011) 981–1014, https://doi.org/10.1016/j.progpolymsci.2011.02.001.

[43] Q. Li, P. Zhang, Y. Cai, Genkwanin suppresses MPP+-induced cytotoxicity by inhibiting TLR4/MyD88/NLRP3 inflammasome pathway in a cellular model of Parkinson's disease, NeuroToxicology 87 (2021) 62–69, https://doi.org/10.1016/j.neuro.2021.08.018.

[44] C.J. Lawrimore, F.T. Crews, Ethanol, TLR 3, and TLR 4 agonists have unique innate immune responses in neuron-like SH - SY 5Y and microglia-like BV 2, Alcoholism Clin & Exp Res 41 (2017) 939–954, https://doi.org/10.1111/acer.13368.

[45] C. Qiao, L.-X. Zhang, X.-Y. Sun, J.-H. Ding, M. Lu, G. Hu, Caspase-1 deficiency alleviates dopaminergic neuronal death via inhibiting Caspase-7/AIF pathway in MPTP/p mouse model of Parkinson's disease, Mol. Neurobiol. 54 (2017) 4292–4302, https://doi.org/10.1007/s12035-016-9980-5.

[46] L. Aloe, M. Rocco, B. Balzamino, A. Micera, Nerve growth factor: a focus on neuroscience and therapy, CN 13 (2015) 294–303, https://doi.org/10.2174/1570159X13666150403231920.